



Cite this: *Soft Matter*, 2017, **13**, 776

Stretching-induced wrinkling in plastic–rubber composites†

Junyu Yang,^{‡a} Sameer Damle,^{‡a} Spandan Maiti^b and Sachin S. Velankar^{*a}

We examine the mechanics of three-layer composite films composed of an elastomeric layer sandwiched between two thin surface layers of plastic. Upon stretching and releasing such composite films, they develop a highly wrinkled surface texture. The mechanism for this texturing is that during stretching, the plastic layers yield and stretch irreversibly whereas the elastomer stretches reversibly. Thus upon releasing, the plastic layers buckle due to compressive stress imposed by the elastomer. Experiments are conducted using SEPS elastomer and 50 micron thick LLDPE plastic films. Stretching and releasing the composites to 2–5 times their original length induces buckles with wavelength on the order of 200 microns, and the wavelength decreases as the stretching increases. FEM simulations reveal that plastic deformation is involved at all stages during this process: (1) during stretching, the plastic layer yields in tension; (2) during recovery, the plastic layer first yields in-plane in compression and then buckles; (3) post-buckling, plastic hinges are formed at high-curvature regions. Homogeneous wrinkles are predicted only within a finite window of material properties: if the yield stress is too low, the plastic layers yield in-plane, without wrinkling, whereas if the yield stress is too high, non-homogeneous wrinkles are predicted. This approach to realizing highly wrinkled textures offers several advantages, most importantly the fact that high aspect ratio wrinkles (amplitude to wavelength ratios exceeding 0.4) can be realized.

Received 7th August 2016,
Accepted 17th December 2016

DOI: 10.1039/c6sm01823h

www.rsc.org/softmatter

1. Introduction

A thin stiff elastic film bonded to a softer elastic substrate can buckle to form wrinkle patterns when subjected to compressive stress. The past decade has seen numerous articles in this area exploring the fundamental mechanics of such buckling,^{1–4} and applications such as smart surfaces with tunable adhesion, friction, and wettability, flexible electronics, and thin film metrology.^{5–12} A large majority of research has examined elastic systems, *i.e.* the thin films as well as soft substrates were treated as elastic (often linearly elastic) materials.^{1,3,13,14} But materials used in experiments or materials of interest to practical applications often have more complex properties, and there is now a growing literature on thin film wrinkling when the substrate or film is an inviscid liquid,^{15–17} viscous liquid,^{18–21} viscoelastic,^{22–24} capable of yielding,^{25–27} or softening upon increasing temperature.²⁸ It is in this spirit that the current paper examines the deformation and wrinkling

behavior of films comprising a hyperelastic rubber and yielding plastic sheets bonded to each other.^{29,30}

The essential idea, illustrated schematically in Fig. 1A, appears in a previous patent.²⁹ Fig. 1B shows a dogbone specimen of a trilayer film. The mid-layer of this composite film is a styrene–ethylene/propylene–styrene (SEPS) rubber of 860 micron thickness. It is bonded to two face layers of linear low density polyethylene (LLDPE), each 50 micron thick. This trilayer sample was stretched to a nominal strain of 200%, and then released, upon which the surface developed strong permanent wrinkles (Fig. 1C and D). Fig. 1E shows the wrinkle pattern replicated in silicone rubber (details in the experimental section below). The mechanics underlying this stretch-and-release induced wrinkling have been previously explained as follows:^{29,30} the LLDPE polymer comprising the face layers is known to undergo irreversible plastic deformation upon stretching. In contrast, the SEPS elastomer in the mid-layer stretches reversibly. Thus, upon stretching, a large geometric mismatch is created: the stress-free length of the face layers is longer (roughly by two-fold) than the stress-free length of the elastomer. Thus upon releasing, the elastomer imposes a compressive stress on the face layers. Being much thinner and stiffer than the elastomer, these face layers then buckle into a wrinkle pattern. In the simplest interpretation,³⁰ the situation immediately prior to release is analogous to that observed in the numerous citations at the beginning of this paper:^{1–12} a longer

^a Dept. of Chemical and Petroleum Engineering, University of Pittsburgh, Pittsburgh, PA 15261, USA. E-mail: velankar@pitt.edu

^b Dept. of Biomedical Engineering, University of Pittsburgh, Pittsburgh, PA 15261, USA

† Electronic supplementary information (ESI) available. See DOI: 10.1039/c6sm01823h

‡ Junyu Yang and Sameer Damle are joint first author.

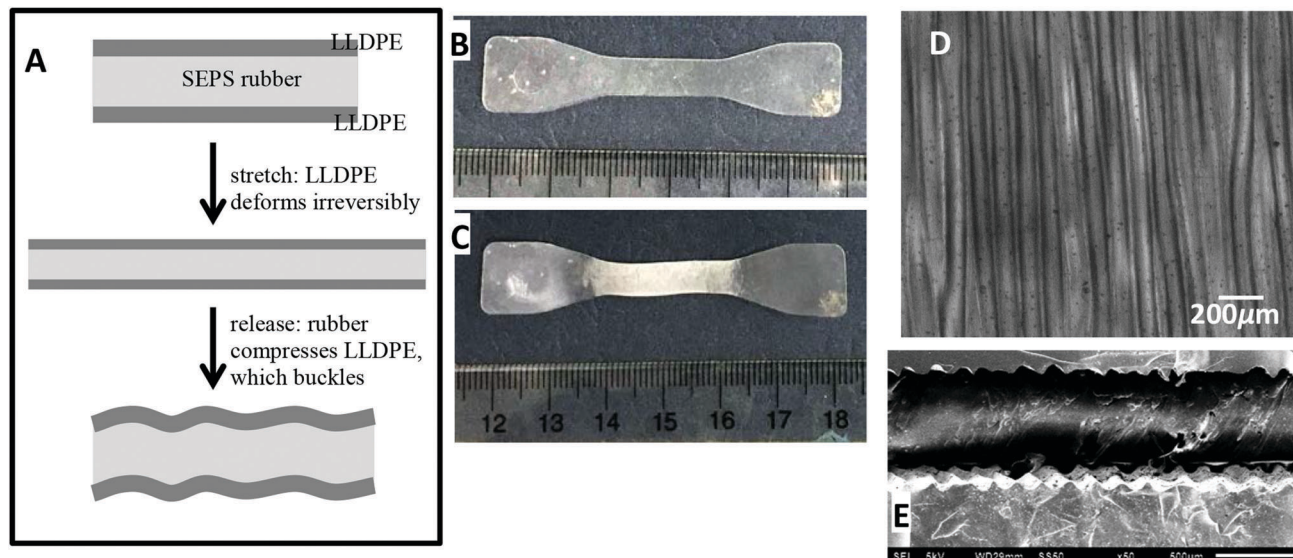


Fig. 1 (A) Schematic representation of the experiment; images of (B) a sample before stretching, and (C) the same sample after stretching; (D) an optical microscope image of the wrinkled surface; (E) SEM image of the cross sectional profile of the sample replicated in silicone rubber.

stiffer elastic film, bonded to a shorter, softer, elastic substrate. Thus, upon release, wrinkles appear due to the competition between the elastic energy of bending the film *vs.* the elastic energy of deforming the rubber. We will show that this interpretation, which is entirely based on purely elastic deformations, is overly simplistic.

The idea of stretching a plastic–elastic composite to create geometric mismatch appears to be generalizable to many different plastics, and the patent by Krueger *et al.*²⁹ cited examples of other pairs of elastomers and polyolefin plastic face layers that gave similar results. Later Hu *et al.*³⁰ conducted elegant experiments of stretch-release-induced buckling, except that in their case, the thin plastic layer (polypropylene, PP) was sandwiched between two thick elastomer face layers (SEPS). An article by Takei *et al.*³¹ published very recently after this research was completed shows the same idea being implemented with bilayers composed of silicone elastomer as the elastic layer and either vapor-deposited parylene or a fluorinated polymer as the plastic film. These latter researchers focus more specifically on the formation of high aspect ratio “ridge” wrinkles. Yet another article by El Haitami *et al.*²⁸ has examined polychloroprene rubber samples whose surface was brominated by a chemical treatment. Due to this treatment, within a few-micron-thick region near the surface, the glass transition temperature exceeded room temperature. Thus stretch-and-release at 20 °C led to formation of wrinkles because these near-surface glassy regions could maintain their deformation. Neither of these latter papers^{28,31} appear to have known about the previous research by Krueger *et al.*²⁹ and Hu *et al.*³⁰

Beyond the experimental observations, Hu *et al.*³⁰ also developed a model for the buckling process and for the wavelength of the buckles. However the model had significant deficiencies. Most importantly, the materials were treated as being elastic during release; the only role of plasticity was to

allow irreversible stretching, hence creating a geometric mismatch between the plastic and elastic layers. In fact this article will point out that film plasticity plays a dominant role at all stages: stretching, recovery prior to buckling, and post-buckling. Thus an elasticity-based model is altogether unsuitable, a conclusion that likely applies not just to the stretch-and-release situation considered here, but to all thin film wrinkling problems where plastic deformation occurs.

While this paper does not explore practical applications for such wrinkled composites, in fact this stretch-and-release approach offers many practical advantages: (1) the materials (LLDPE and synthetic rubber, especially polyolefin elastomers) are inexpensive, and thus viable for large volume applications such as superhydrophobic packaging. (2) The plastics industry routinely produces multilayer films with tens of layers, and hence such films can be mass-produced by coextrusion. (3) The plastics industry can realize layer thicknesses in the sub-micron range, and thus buckles with micron-scale wavelength and amplitude can be realized. (4) The buckles can have high aspect ratio; an amplitude to wavelength ratio of 0.4 is reached in this paper (0.5 was achieved by the ridge-wrinkles of Takei *et al.*³¹). In contrast, it is generally difficult to reach such aspect ratios exceeding 0.3 with elastic wrinkles. A notable exception is Chen and Crosby,³² who achieved an aspect ratio of 0.65 with careful material selection (that paper also provides citations to previous literature on lower aspect ratios). (5) Polyolefins with a vast range of moduli and yield stresses are available, thus permitting tuning of the wavelength and amplitude. (6) Many such material pairs have excellent mutual adhesion, and the adhesion can be improved further by compatibilizers.^{33–35} Thus delamination – a common consequence of internal stresses in layered composites – can be readily avoided. These advantages for practical applications are in contrast to the drawbacks of these materials for lab-scale experiments: (1) coextrusion, which is well-suited for large-scale

manufacturing of thermoplastic polymers, is extremely ill-suited for small-scale sample preparation because highly specialized equipment is needed, (2) films of materials such as LLDPE or other semi-crystalline polyolefins cannot be prepared by methods such as spin-coating or vapor deposition whose simplicity makes them popular in the soft materials community, and (3) as a consequence, it is difficult to prepare samples with a variety of film thickness (in our paper, a single film thickness from a commercial manufacturer is used). These disadvantages may be one reason why there is only limited research on wrinkling of such bilayers.

In summary then, the motivation for this paper is twofold. First, the mechanical picture proposed previously, which interprets wrinkling in terms of elastic deformations, is overly simplistic. Instead we show that more recent research on plasticity effects in similar layered geometries^{26,27,36,37} is much more relevant to understanding and controlling the stretch-and-release process. More specifically, the distinctive features of plastic deformation, *e.g.* necking in tension or plastic hinge formation in bending, play a crucial role in such situations. Second, the patent on stretching-induced wrinkling of plastic-elastomeric multilayers dates back to 1997, and the research article by Hu *et al.*³⁰ to 2004. Yet, this simple idea of creating wrinkled surfaces has received very little attention – despite the enormous research on various other aspects of thin film buckling over the past 15 years. In light of the potential advantages mentioned in the previous paragraph, further research on the underlying mechanisms may bring this method into wider practice.

The outline of this paper is as follows. Section 2 describes the materials and methods. Section 3 discusses the mechanical behavior of trilayers and the effect of stretching strain on the wavelength and amplitude of buckles. The experiments in this section roughly follow Hu *et al.*;³⁰ however, in the analysis, we emphasize the importance of examining the data in terms of the local stretch (rather than nominal strain) since plastic materials are prone to non-homogeneous deformation (*e.g.* necking, Fig. 3A). Section 3 will discuss why a purely elastic model is insufficient and argue in favor of a more detailed consideration of plasticity. Section 4 conducts numerical simulations treating the face layers as an elasto-plastic material, and the SEPS as a hyperelastic material.

2. Methods

2.1. Experimental

Many of the experimental details are provided in Section S1.1 of the ESI,[†] and only the important points are listed here. The rubber used was Kraton G1730 SEPS triblock copolymer with a modulus of 3.3 MPa. The LLDPE films were commercial films of 50 micron thickness. Trilayers were prepared by compression molding the rubber pellets between sheets of the LLDPE films and cut into dogbone shapes (20 mm gauge length) for tensile testing. Samples were stretched in a MTS testing machine to the desired strain (50% to 300% at a rate of 100% per minute based

on the nominal test length). Immediately after reaching the desired strain, the samples were allowed to contract at the same rate, a step dubbed “release”. The entire tensile tests were video-recorded and actual strains were obtained from displacement of ink markers placed on the sample surfaces.

Determining the wrinkle profile requires an edge-on view of the wrinkles. However, it is not possible to cut the films without inducing large plastic deformation as explained in Section S1.1 (ESI[†]). Therefore the wrinkle profile was reproduced in silicone as follows. The samples (recovered after tensile testing) were embedded in a liquid silicone rubber precursor (Sylgard 184) which was allowed to cure, thus replicating the sample topography in silicone. Since the silicone does not adhere strongly to LLDPE, the samples could readily be pulled away from the rubber, the silicone rubber cut, and imaged by optical or scanning electron microscopy. Due to this replication procedure, Fig. 1E represents the “negative” of the wrinkled surface profile of the original samples.

Finally, the geometric mismatch induced in these samples is severe, and hence delamination is a potential concern. We verified (see Section S1.2 in ESI[†]) that delamination does not affect our experiments.

2.2. Simulation

A custom-developed nonlinear 3D finite element analysis program was used to conduct all the FE analyses in this article. This suite of software has previously been used to simulate the mechanical behavior of various biomaterials and advanced energy materials.^{38–41} A variety of material behaviors can be simulated using this computational platform. The details of the constitutive models used for plastic and elastomeric layers can be found in Section S2 of the ESI.[†]

A schematic representation of the cross-section of the trilayer sample is shown in Fig. 2A. In the experiments (Section 3.1) the

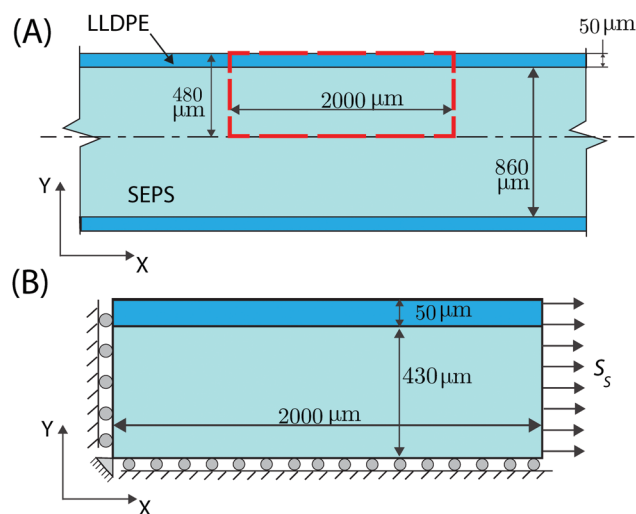


Fig. 2 (A) Cross-section of the trilayer sample. The dashed red rectangle denotes the domain selected for finite element simulation. (B) Boundary conditions for the finite element simulations of loading and unloading of the trilayer sample computational domain.

deformation is localized at the central gauge length of the dogbone sample, while the wider ends of the sample near the clamp experience much less strain. Thus, a small section in the central part of the trilayer sample (length 2 mm and width 0.1 mm) was taken for computational modeling purposes. Furthermore, due to the symmetry of the trilayer sample in the thickness direction (Z direction), only the upper half of the specimen (marked by the dotted red rectangle in Fig. 2A) was considered for all the simulations. The computational domain was meshed with 6200 hexahedral elements using Trellis Pro 15 (csimsoft, American Fork, UT).⁴²

Boundary conditions used for the model are indicated in Fig. 2B. Surfaces of the domain parallel to the plane of the paper were placed on rollers to eliminate their out of the plane motion. In addition, roller boundary conditions were applied to the left surface and the bottom surface to exploit the symmetry of the domain. A local stretch of 2.86 was applied first on the right surface, incrementing linearly over 10 000 load steps. The reason for selecting this value of stretch will be mentioned in Section 4. Upon completion of the loading phase, random perturbations were applied at the finite element nodes of the LLDPE layer mesh in the Z direction, not exceeding 0.5% of the thickness of the LLDPE layer. Next, the applied stretch at the right surface was released (*i.e.*, reduced from 2.86 to 1.0) in 10 000 load steps. Reaction forces at each FE node on the left surface were recorded at each loadstep. These forces were summed over all nodes on that surface and the result divided by the undeformed area of that surface to obtain the first Piola-Kirchhoff stress used to plot the stress-strain curve for the specimen. Visualization of the stress and strain contours is done using the ParaView software.⁴³

The overall goal of the simulations is not to capture the quantitative details of the deformation and wrinkling process, but to explore qualitatively the mechanical phenomena that are

important to produce surface instabilities during stretching and subsequent release of the thin film. Accordingly, we used the simplest constitutive behavior that can capture the pure component behaviors of the rubber and the plastic layers. The rubber was modeled as a 2-parameter Mooney–Rivlin material. The material parameters $C_1 = 85$ kPa and $C_2 = 475$ kPa were obtained by fitting the experimentally measured stress response of dogbone samples of the rubber to the stress response of the Mooney–Rivlin model (see eqn (S10), ESI†). The Poisson's ratio of the rubber was set to 0.499. The LLDPE face layer was modeled as a neoHookean material up to the yield point, and behaved as a perfectly plastic material after yielding, *i.e.*, maintained a stress equal to the yield strength without any strain hardening. The constitutive response of the face layer was captured by two parameters: the elastic modulus prior to yield, E_{plastic} (set to 400 MPa in all simulations), and the yield strength, σ_y (set to 10 MPa unless specified otherwise). These parameters combine to provide a yield strain of approximately 2.5%. We assumed that the deformation gradient \mathbf{F} admits a multiplicative decomposition into a plastic and an elastic part. The yield function $f(\mathbf{M}_e)$ was written in terms of the deviatoric part \mathbf{M}_e^d of the Mandel stress tensor \mathbf{M}_e defined in the intermediate configuration as $f(\mathbf{M}_e) = \sqrt{\frac{3}{2}\mathbf{M}_e^d:\mathbf{M}_e^d} - \sigma_y = 0$, where σ_y is the yield strength.

Details of the implementation can be found in the ESI.†

3. Results and discussion

3.1. Mechanical behavior

Fig. 3 illustrates the tensile behavior of the rubber, the plastic, and the trilayer, along with the images extracted from videos of

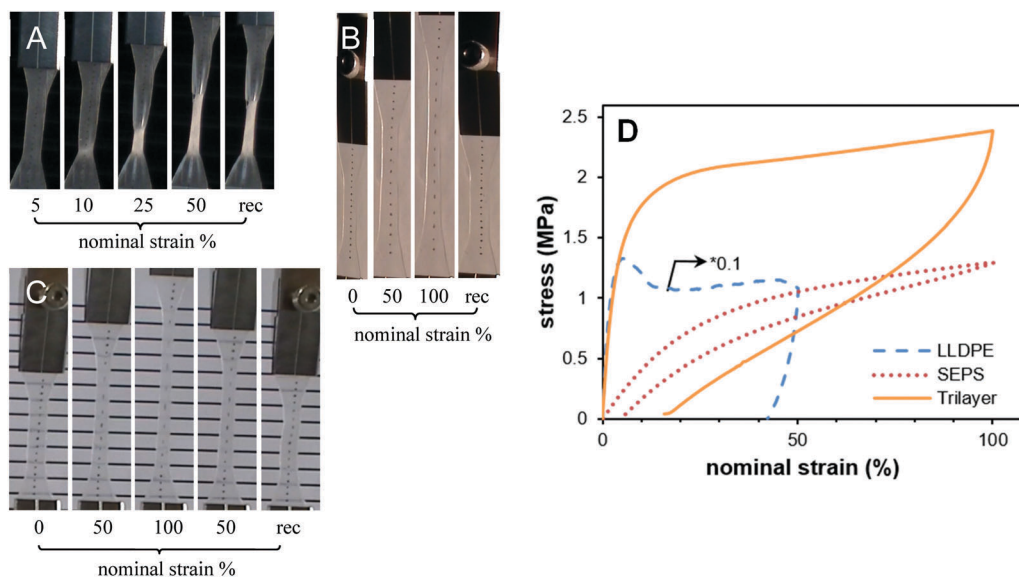


Fig. 3 Images extracted from videos of the stretching dogbone specimens of (A) LLDPE, (B) SEPS, and (C) trilayer with an 860 micron SEPS midlayer. Nominal strains are noted below each image. “rec” denotes the final recovered state when the stress is nearly zero. In (B and C), black ink marks are made on the specimens to track local strain. In (C), a ruled sheet of paper was placed in the background to help identify the edge of the specimen. (D) Engineering stress vs. nominal strain for all three samples. The data for the LLDPE have been multiplied by a factor of 0.1.

the process. Here the nominal strain, $\epsilon_{\text{nominal}}$, on the x -axis is simply the change in the length of the dogbone sample (displacement of the crosshead of the testing platform) relative to the original sample length. The tensile data for SEPS (Fig. 3D) show behavior typical of elastomers: a low modulus (3.3 MPa) during stretching, and only modest hysteresis during recovery, with an unrecovered strain of a few percent. The corresponding video frames (Fig. 3B) show that the strain is homogeneous.

The LLDPE shows behavior typical of a semicrystalline polymer: a modulus of ~ 400 MPa, followed by yielding at a few percent strain. Note that the stress of the LLDPE has been scaled by a factor of 0.1 in Fig. 3D. The corresponding images from videos (Fig. 3A) show that the yielding is accompanied by strong necking, and as deformation increases, the neck grows by drawing in the surrounding material. Despite the stability of the neck, the plastic layer typically fails at less than 70% nominal strain. Accordingly, in Fig. 3, the sample was only stretched to 50% nominal strain before reversing the stretching. During recovery, strong hysteresis is evident, with the force dropping rapidly to zero with very little recovery. Indeed the video shows that this small recovery corresponds to the portion of the sample that was not necked; the necked region itself shows negligible recovery (too small to be measured by our video imaging).

The behavior of the trilayer combines characteristics of both the rubber and the plastic: on one hand there is large hysteresis in stretching *vs.* recovery. On the other hand, the deformation is homogeneous with no apparent necking, and the sample recovers its original length almost completely.

Fig. 4 shows the stress–strain curves as the maximum applied nominal strain is varied from 50% to 300%. The early portion of the stretching curves is an indicator of the typical sample-to-sample variability. All the qualitative features noted above apply at all these strains: (1) at all these strains, samples did not show any apparent non-homogeneity or necking during stretching; (2) at all strains, there is significant hysteresis in the stretching *vs.* release curves, (3) yet all recover a considerable

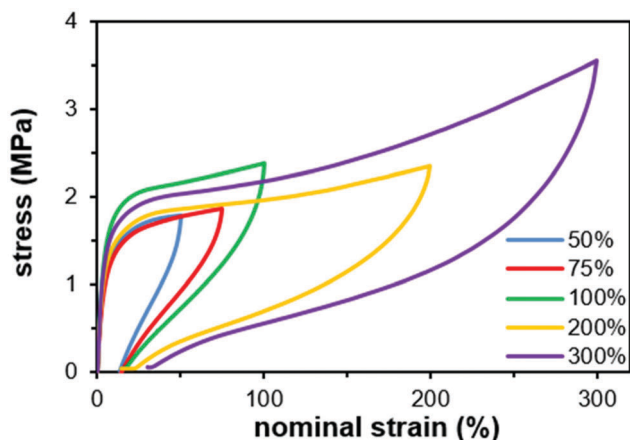


Fig. 4 Engineering stress *vs.* nominal strain for the trilayer samples with an 860 micron SEPS midlayer.

portion of the applied deformation. Quantitatively however, it is apparent that the irreversible deformation increases with the applied deformation. Similar experiments were conducted for the SEPS itself, and the corresponding results, in the form of load *vs.* elongation, will be presented in Fig. S8 (ESI \dagger) later.

From a fundamental perspective, the actual local strain is more relevant than the nominal strain, and hence it is more useful to express all results in terms of the local stretch, S . All the relevant geometric quantities are defined in Fig. 5A, which illustrates the samples at four important points along the deformation path: the initial condition, the point of maximum stretching when the stretch is S_s , the critical point at which wrinkles first appear at a critical stretch of S_c , and the final recovery when the stress drops to zero at the stretch S_r . Fig. 5B and C compare the local stretch values, from video analysis, for the rubber and the plastic at the end of the stretching step (S_s), and at the end of the recovery step (S_r). A few points are noteworthy. First, the local stretch S_s in Fig. 5B is larger than $(1 + \epsilon_{\text{nominal}})$, presumably because the wider end-sections of the dogbone stretch much less than the gauge section. Second, from Fig. 5C, the rubber recovers almost completely, with a less than 10% change in length even after being stretched to five times its original length. Third, from Fig. 5C, the irreversible deformation S_r of the trilayers increases with S_s , as already remarked above.

Limited video analysis of the stretching of free-standing LLDPE films (Fig. 3A) was also conducted, and shows that the stretch of the necked region reaches 4 at very small nominal strain, with only a slight increase with a further increase in nominal strain. The recovery of the necked region is negligible (*i.e.*, cannot be estimated reliably by video analysis).

We now turn to the surface wrinkling phenomenon which motivated this research. At the lowest nominal strain tested, 50%, at the end of the recovery, the dogbone samples appear smooth with no visible wrinkles. Above 70% nominal strain, wrinkles are readily visible, but they are not uniform and certain regions of the dogbone samples may appear smooth. For strains exceeding 100%, the entire gauge section of each dogbone sample appears uniformly wrinkled. Fig. 6A shows optical images of the wrinkle profiles. It must be emphasized that these profiles are not cross sections of the samples themselves, but instead silicone replicas of the sample surface far from the edge as described in Section S1.1 of the ESI \dagger . As such, they are negatives, *i.e.* the “peaks” of the original samples appear as “troughs” in the replicas.

From such images, the buckle wavelengths λ_r and amplitudes A corresponding to the recovered samples can be estimated. These are plotted in Fig. 6B and C. Amplitude/wavelength ratios exceeding 0.4 can be realized (Fig. 6D); with the exception of solvent swelling, such large amplitude buckles are difficult to realize by other methods. It is also noteworthy that films supported on soft solid substrates tend to undergo higher order instabilities such as folding or period doubling at large compression.^{1,17} Such complex post-buckling behavior is not evident in these plastic–rubber composites; instead buckles remain roughly monomodal, even though their profiles are not quite sinusoidal. It is apparent, even from cursory examination of the raw images (Fig. 6A), that the

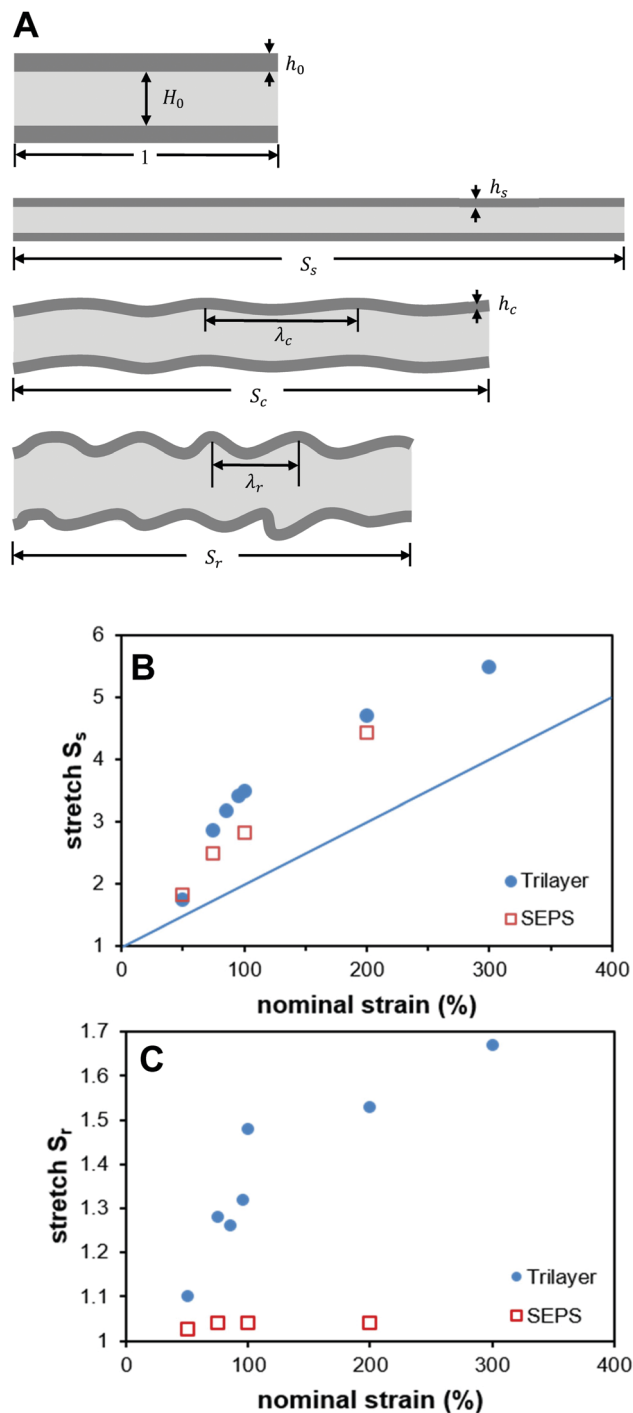


Fig. 5 (A) Definitions of terms. (B) Stretch values at the end of the stretching step, and (C) at the end of the release step.

buckle wavelength reduces with increasing strain. Quantitatively this decrease in wavelength exceeds two-fold (Fig. 6B).

Finally, a limited number of experiments were conducted on trilayers with lower rubber thicknesses, and the corresponding load–strain curves are shown in ESI,† Fig. S2. The overall load reduces with decreasing rubber thickness, but otherwise the shapes of the curves remain qualitatively similar. Despite this apparent similarity as rubber thickness reduces, there is

actually a significant change in deformation behavior: the trilayers with 500 or 860 micron rubber thickness deformed homogeneously; the trilayer with 250 micron rubber thickness showed significantly non-homogeneous deformation, whereas the trilayer with 100 micron rubber thickness showed unambiguous necking (see Fig. S2, ESI†) along the width direction albeit not as severe as the free-standing plastic layers. This is not surprising; with decreasing rubber thickness, there is no longer sufficient rubber to suppress the necking behavior of the plastic face layers. What is surprising is that even with an 8-fold decrease in rubber layer thickness (from 860 to 100 micron), S_r increases very little, and the wavelength of the wrinkles or the wrinkle profile is hardly affected. This is illustrated in Fig. S3 (ESI†) which may be compared with the wrinkle profiles in Fig. 6A in the main text. We regard this as surprising because in a uniaxial tensile experiment, a free standing rubber film of 100 micron thickness develops a maximum force of about 1 N, whereas the force needed to yield the two plastic layers (estimated from the film dimensions and ~ 10 MPa yield strength) is roughly 6 N. Incidentally the latter estimate is well-supported by the dashed line in Fig. 7A presented later. Thus one would expect that such a trilayer would not recover very much, and would not wrinkle. Instead, it is remarkable that the 100 micron rubber layer, which develops only one-sixth of the force needed to induce yielding of the two plastic layers, is still able to recover substantially and induce severe buckling. Indeed Hu *et al.*³⁰ observed similarly weak dependence of wavelength on the rubber/plastic thickness ratio but did not comment on this.

3.2. Elastic model and its limitations

The previous research in this area has interpreted all the results in terms of elastic effects.^{29,30} The essential idea is to think of the film plasticity as having one – and only one – consequence, *viz.* creating a geometric mismatch when the layered composite is stretched. In this picture, during the stretching phase, the plastic layers undergo irreversible deformation, but the subsequent buckling mechanics are entirely interpreted by assuming linearly elastic behavior of both layers. This “elastic-during-release” approach is illustrated in ESI,† Section S3, and it conceptually follows Hu *et al.*,³⁰ except that the stretching-induced thinning of the film is accounted for, and all the analysis is conducted in terms of actual rather than nominal strain. The physical picture is as follows: elastic films supported on softer elastic substrates are known to wrinkle when some critical compressive stress is reached.³ When this critical stress is reached (at a stretch S_c) during release, wrinkles of wavelength λ_c appear everywhere on the film. The wavelength then reduces further as release continues. With the assumptions listed explicitly in ESI,† Section S3, we culminate in eqn (S14), which predicts the wavelength in terms of various geometric parameters and material properties. This equation can reproduce the changes in wavelength with stretching (Fig. S10, ESI†), albeit with one fitting parameter (see Section S3, ESI†).

With a more detailed analysis, further predictions may be made. For instance, if the film is much stiffer but much thinner

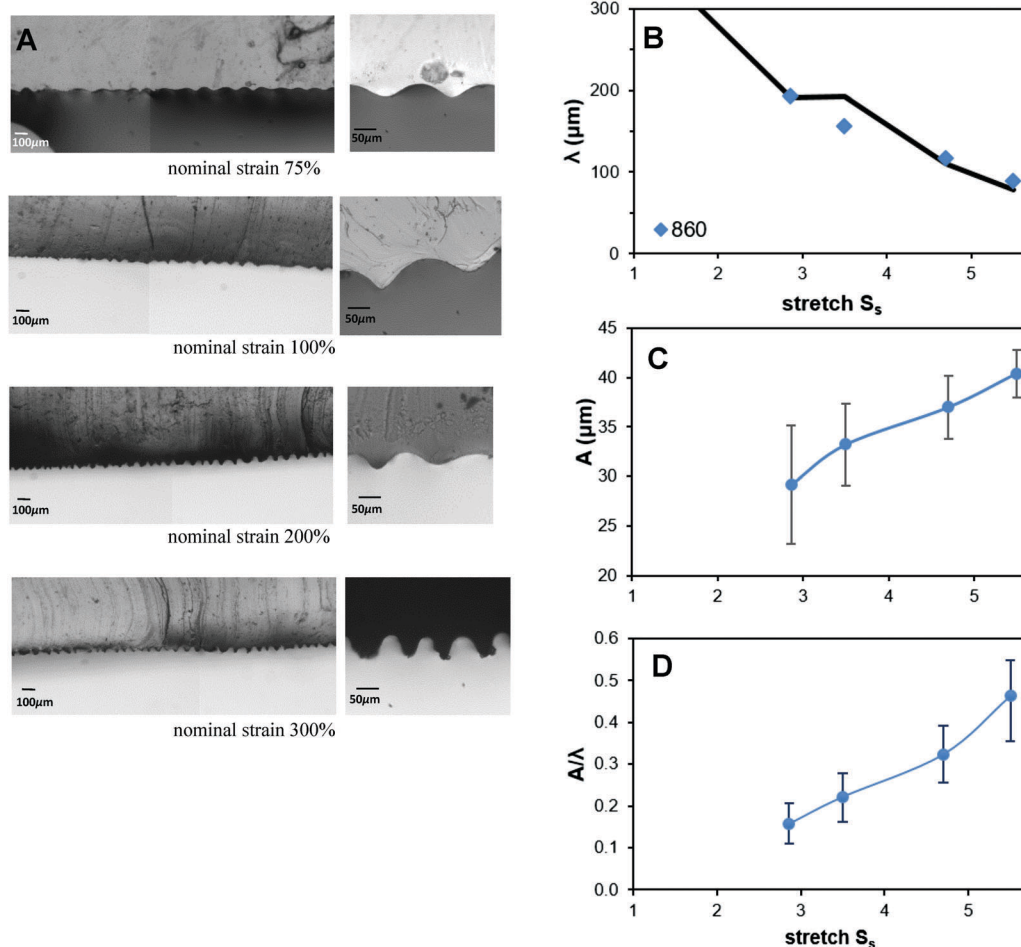


Fig. 6 (A) Images taken by using an inverted microscope: from top to bottom are 100% elongation, 200% elongation and 300% elongation respectively. (B–D) The wavelength, amplitude, and their ratio (A/λ) vs. stretch S_s .

than the rubber layer, one may assume that the contour length of the film is preserved after it buckles, an assumption dubbed “inextensible film” in the wrinkling literature.¹⁷ This would then provide a geometric relationship between amplitude, wavelength, and S_c/S_r . In principle, it is also possible to construct an exact mechanical model which can calculate S_r from minimizing the total energy which is a sum of the stretching energy in the rubber layer and the bending energy of the film.

However these approaches depend on the assumption that the only role of film plasticity is to create a geometric mismatch, and therefore create an internal stress which compresses the face layer. In fact, plasticity can affect the process in many other ways. The first is the possibility of necking during stretching. As explained above, a free-standing LLDPE layer and a trilayer with a 100 micron thick rubber midlayer both undergo obvious necking along the width direction. In contrast, the thickest trilayers (860 micron rubber midlayer) do not. However even for the latter sample, necking along the thickness direction – which would cause the LLDPE layer to become non-uniform in thickness in the fully stretched state – cannot be ruled out. Indeed Li and Suo³⁶ have shown that upon stretching a plastic layer bonded to an elastomeric layer, for certain values of the

geometric and material parameters, the plastic layer undergoes multiple necking, *i.e.* the plastic layer thins at numerous equally spaced locations along the samples. For other parameter values, there was catastrophic necking at one location (*i.e.* the plastic layer failed) or there was uniform thinning of the plastic layer. That research was conducted for the specific case of metal films (which deform plastically) bonded to elastomers, but the same physics is relevant here: the rubber layer “isolates” one region of the film from the other, and hence a single neck does not necessarily dominate the entire sample. If multiple necking does happen during deformation, then during the recovery phase, it is plausible that the thinner regions will buckle first. We have conducted limited experiments to test for this possibility (see Section S1.4, ESI[†]). These experiments suggest that thickness-direction necking does not happen in our samples: instead, the plastic layer undergoes uniform thinning. Nevertheless, depending on the mechanical properties of the rubber and the plastic, non-uniform thinning of the plastic layer may be a possibility. This would violate one of the key assumptions underlying ESI,[†] Section S3.

Second, plasticity may have a large effect during the release step. The face layers experience compressive stress during

release; if this stress exceeds the yield strength, the face layer may yield in compression even before buckling. Yin and Chen²⁶ have examined this situation numerically for biaxial compression and concluded that if the plastic layer yields prior to buckling, the subsequent wrinkle pattern is strongly affected. Indeed our own experiments strongly indicate in-plane yielding: films stretched to 50% nominal strain recover almost completely but do not show wrinkles even though this strain greatly exceeds the yield strain of the plastic. To test for this more directly, we stretched a trilayer film with 860 micron thick rubber to a nominal strain of 200%, but the release was interrupted at a nominal strain of 150% at which no wrinkles appeared. This was followed immediately by re-stretching to 200%. The corresponding load–strain curve (Fig. 7A) shows significant hysteresis upon re-stretching, which may be quantified crudely by subtracting the rubber load from the plastic load (dashed green line in Fig. 7A). In contrast, the free-standing rubber layer shows no significant hysteresis in this same experiment. Thus the likely cause of trilayer hysteresis is that the plastic film accommodates at least a portion of the compressive strain by in-plane yielding rather than wrinkling. Other potential mechanisms, *e.g.* some dissipative processes of interfacial failure, cannot be ruled out.

Third, the elastic model in ESI,[†] Section S3, presumed plane-strain conditions, whereas the experimental samples have only a modest width with no constraints along the edge direction. Accordingly, during the release step, the trilayer

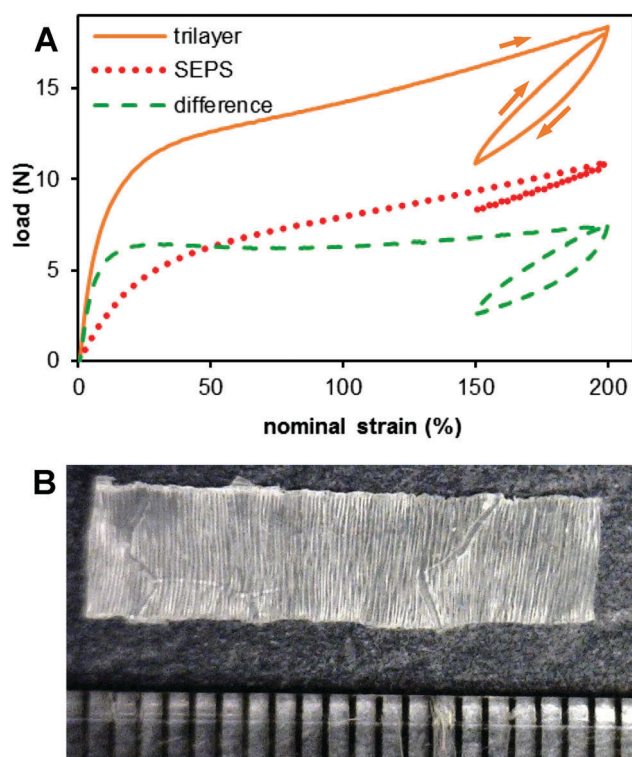


Fig. 7 (A) Partial release followed by restretching for a trilayer and SEPS rubber. The dashed green line is a point-wise subtraction of the SEPS and the trilayer. (B) Image of one of the LLDPE plastic face layers recovered after dissolving the SEPS elastomer in toluene. Each marking on the ruler corresponds to 1 mm.

sample increases in width. If the rubber is sufficiently thick, the kinematics of this deformation correspond to unidirectional compression, and therefore the width would increase by a factor of $\left(\frac{S_s}{S_r}\right)^{0.5}$ during the entire release step. The corresponding strains far exceed the $\sim 2\%$ yield strain of the plastic layer, *i.e.* the face layers may stretch irreversibly in the perpendicular direction during recovery.

Finally, after wrinkling, there may be localized plastic deformation at the points of highest curvature. Since the deformation is tensile on one surface of the plastic layer, and compressive on the opposite face of the same layer, the plastic layer is expected to yield in bending and form plastic hinges. The simulations of Takei *et al.*³¹ indicate that such plastic deformation leads to an increase in curvature and a narrowing of ridges. To test for this possibility, samples stretched to 200% nominal strain were immersed in toluene, a solvent which dissolves the rubber mid-layer, but leaves the face layers undamaged. Fig. 7B shows a photo of the plastic face layers recovered from this experiment and it is clear that they maintain their ruffled appearance and do not relax back to a flat state. Similar ruffles are evident in Fig. S1 (ESI[†]) when the LLDPE face layers are no longer bonded to the elastomer; in that case the solvent was not needed since the films spontaneously delaminated at the sample edges. Both these images establish beyond doubt that the films do not behave elastically during release, and that plastic hinges are formed. To what extent they influence the mechanics is difficult to establish experimentally. Incidentally we note that for very small film thicknesses, such plastic deformation may appear at much smaller strains than expected from their bulk behavior.³⁷

In summary, while treating the layers as elastic provides a qualitative explanation of why wrinkling appears, plastic deformation is expected to have significant consequences even during the release step. Clear insight into the factors driving the buckling requires a much more detailed consideration of how plastic deformation occurs. For this we turn to numerical simulations.

4. Simulations

4.1. Wrinkle formation

Fig. 8 shows the stress vs. stretch curve obtained from the simulations for the trilayer and for the rubber layer. These simulations are conducted with the material properties listed in the last paragraph of Section 2.2, with the rubber modulus being 3.3 MPa and the plastic yield strain being 10 MPa. Snapshots of the simulation at points labeled A–H are presented in Fig. 9. The stress in the rubber layer increases monotonically during stretching, and recovers without hysteresis during release. The stress–strain behavior for the trilayer is dominated by the plastic layer at very small deformation until the plastic layer starts yielding at a strain of 2.5% (corresponding to the abrupt change in the slope of the stress–strain curve). During the release step, there is pronounced hysteresis consistent with experiments: the stress first drops sharply until the

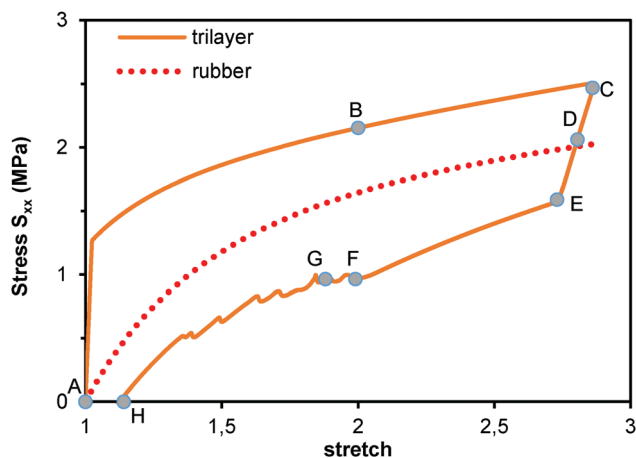


Fig. 8 Stress vs. stretch curves obtained from the finite element simulation. The points marked with solid circles correspond to the snapshots in Fig. 9.

plastic layer yields in compression at point E (see below) and then more gradually to the zero stress state (point H). Qualitatively consistent with the experiments, the overall stress reduces to zero when the strain is still positive. The actual value of S_r in simulations is smaller than the experimental value, although it must be recognized that this is true for the rubber layer too; the experiments show $S_r \sim 1.05$ for the SEPS layer by itself, whereas the simulations of course show $S_r = 1$, a consequence of ignoring irreversible deformation of the rubber layer.

Fig. 9 shows snapshots at various points during the stretching (to $S_r = 2.86$) and subsequent release of the trilayer film. This value of 2.86 roughly corresponds to the actual stretch in

the 75% elongation experiment. The distributions of the Cauchy stress S_{xx} (eqn (S5), ESI†) are shown as colormaps. During the stretching step, both layers thin uniformly (this will be discussed further later). As expected from the constitutive equation, the plastic layer yields at a stretch of roughly 1.025 (not shown), and thereon for the remainder of the stretching step, the stress in the plastic layer remains constant at σ_y .

Upon release, the initial recovery behavior is as expected: the stress in the plastic layer reduces elastically, reaches zero at $S = 2.805$ (Fig. 9D), and subsequently becomes compressive. However when the compressive stress reaches σ_y at a stretch of 2.73 (Fig. 9E), the plastic layer starts yielding in compression. Upon further release, at a stretch of about 1.99, wrinkles appear. It is remarkable that there is a large range of stretch (from 2.73 to 1.99) within which the film accommodates the compression by yielding in-plane without developing wrinkles. Once wrinkles appear, they grow as the film recovery continues and the simulation is stopped at $S_r = 1.13$ when the net load in the computational domain reaches zero. The non-uniformity of the wrinkle growth is striking: some buckles grow to a large amplitude much earlier than others. The random thickness variation in our computational model may have introduced the heterogeneity responsible for growth of localized folds as suggested by Semler *et al.*,⁴⁴ albeit for purely elastic systems. This apparent non-homogeneous growth of wrinkles resembles the “ridge” mode explored previously^{14,45,46} where tall localized ridges appear in elastic/elastic bilayers when the substrate is prestretched. However in that case, the wrinkles surrounding each ridge tend to reduce in amplitude when a ridge is formed, a feature that is not evident in Fig. 9. Despite the simple model of plasticity and the plane strain assumption, the average

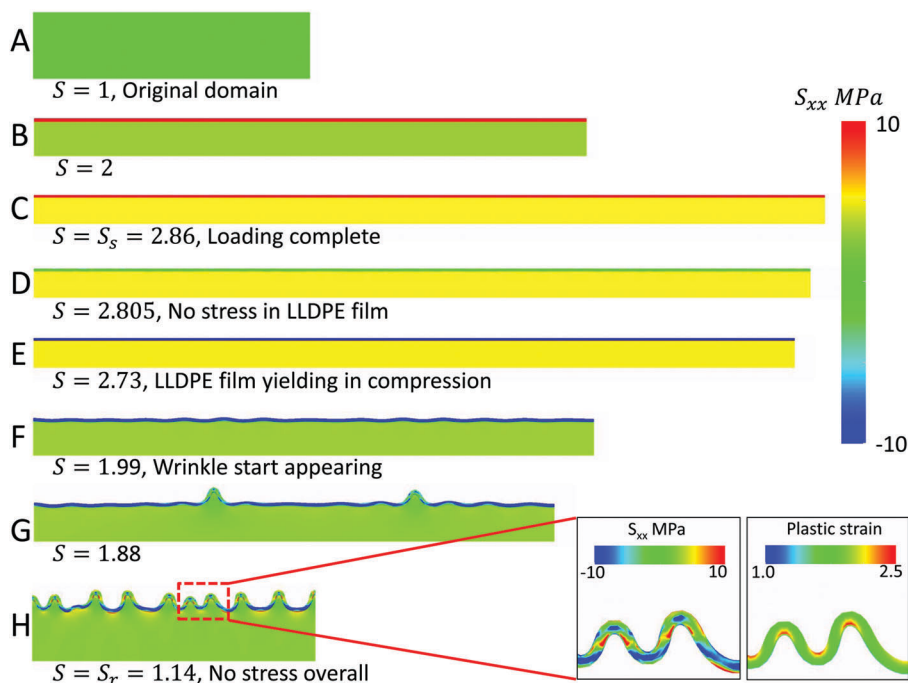


Fig. 9 Snapshots of the domain during loading and unloading simulation. The yield strength of plastic film is 10 MPa. Contours of S_{xx} stress are shown.

spacing between the simulated wrinkles (~ 230 micron) is close to that observed experimentally (~ 180 micron) at a similar stretch.

The inset of Fig. 9 examines in greater detail the Cauchy stress S_{xx} and the local plastic strain in the film at the end, *i.e.* at $S_r = 1.13$. It is immediately apparent that film bending induces differential yielding along the thickness direction. While the film as a whole is under compressive load, the outer surface of the film at the crest of the wrinkles experiences tensile stress and thus yields in tension. On the other hand, the inner surface of the film at the film–rubber interface is under compressive stresses. The stress state is opposite at the troughs with tensile and compressive stresses at the inner and outer surfaces, respectively. Thus, there are large plastic strain gradients through the thickness of the film at the peaks and troughs of the wrinkles giving rise to “plastic hinges” at these locations. These hinges cause the shape of the wrinkles to deviate from the sinusoidal profile common in elastic material systems, and permit the development of high aspect ratio wrinkles.

It is noteworthy that the simulations contradict all of the assumptions of the elastic model³⁰ of ESI[†] Section S3: (1) eqn (S1) (ESI[†]) assumed that wrinkles appear when both materials are elastic, whereas the simulations suggest that the face layer yields prior to buckling; (2) eqn (S12) (ESI[†]) assumed that the film thickness remains at h_s during release whereas simulations suggest that the film thickens as it yields prior to buckling; (3) wrinkles were assumed to grow uniformly everywhere, whereas the simulations show that some buckles grow much earlier than others; (4) eqn (S13) (ESI[†]) assumed that the existing buckles simply reduced in wavelength (and increased in amplitude) while remaining roughly sinusoidal, whereas in the simulation, the wrinkle profiles show highly localized curvature; (5) finally, the physical picture of ESI[†] Section S3, assumed that the film experienced compressive strains everywhere, whereas the formation of plastic hinges in the inset of Fig. 9 indicates that at some locations, the film undergoes large tensile deformation.

Finally, a limited number of simulations were conducted to find the stretch at which in-plane yielding gives way to wrinkling, as the material properties change. The table in ESI[†] Section S2.4, shows that this stretch reduces as the yield strength σ_y reduces at a fixed rubber modulus. At a yield stress of 3.5 MPa, the entire release process is accommodated by in-plane yielding. Thus the simulations indicate that there exists a minimum yield stress that is needed for the stretch-and-release process to induce wrinkles.

4.2. Necking behavior during stretching

Finally we discuss the behavior predicted by simulations if the parameter values were slightly different than used in Fig. 9. Specifically, Fig. 9 assigned a yield strength value of 10 MPa to the plastic film whereas the measured value for LLDPE (Fig. 3D) was slightly higher. In fact our initial simulations, which used a value of 12.5 MPa, showed qualitatively different behavior illustrated in Fig. 10. Fig. 10A–E show the snapshots of the simulation domain during stretching of the trilayer using a yield strength value of 12.5 MPa. The remaining properties were

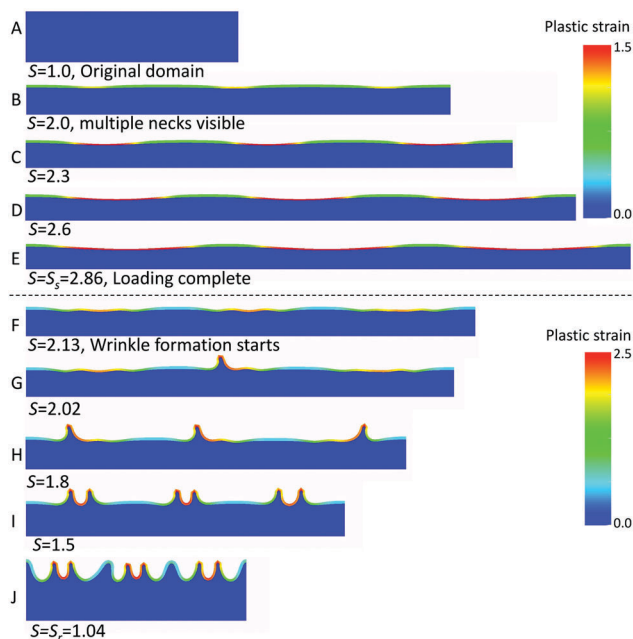


Fig. 10 Snapshots at various stretch values during loading and unloading simulation. The yield strength of plastic film is 12.5 MPa. (A–E) Loading of the trilayer domain and (F–J) unloading. Contours of plastic strain are shown. Note that the plastic strain scale bar for (A–E) is different from that for (F–J).

kept the same as reported in Section 2.2, *i.e.* the yield strength is the only difference between Fig. 9 and Fig. 10. At this value of yield strength, the stretching behavior is quite different: the plastic layer shows strain localization as evidenced by formation of necks (along the thickness direction since this is a plane strain simulation). The strain localization is first observed during the loading of the trilayer at $S_r = 1.78$ (not shown in Fig. 10). Upon increasing the stretch, the plastic strain becomes localized at these necks (Fig. 10B–E). In Fig. S5 (ESI[†]), the thickness of the plastic layer is plotted along the reference length of the simulation domain at four different stretch values. It is evident that upon increasing the stretch, necking becomes increasingly severe (*i.e.* the magnitude of thickness variations increases as the stretch increases). This non-uniform thickness strongly affects the subsequent release step (see Fig. 10F–J). Wrinkles can be seen to first appear at the thinner locations of the film, and only after these initial wrinkles nearly reach their final amplitude do the thicker regions start developing wrinkles.

Additional simulations were conducted to investigate the necking behavior as the yield strength was varied. Fig. S6 (ESI[†]) shows the results of the trilayer films with various yield strength values between 5 MPa and 30 MPa, and simulation snapshots shown at stretch values slightly larger than those at which non-uniform thinning became apparent. All films with $\sigma_y > 12.5$ MPa show non-uniform thinning of the face layer which becomes increasingly severe as the yield strength increases: not only does the width of the neck increase, but furthermore, the strain at which necking is initiated also reduces. It appears

therefore that the experimental value of $\sigma_y \approx 12.5$ MPa is, fortuitously, very close to the minimum value at which periodic necking appears in the simulations.

We have conducted experiments on films stretched to a stretch of roughly 2 to test whether such periodic necking or any kind of non-uniform thinning indeed appears experimentally. These experiments, described in Section S1.4 of the ESI,[†] showed no evidence of non-uniform thinning. This immediately raises the question of why the simulations readily show periodic necking when the experiments suggest that the thinning is homogeneous. We believe that the central reason for this is that the constitutive behavior used for the plastic layer is overly simplistic. Specifically, LLDPE, like most semicrystalline polymers, shows pronounced strain hardening after yielding.⁴⁷ The micromechanical reason for this is that semicrystalline polymers have a significant content of amorphous chains tying together the crystallites, and these amorphous regions behave like typical elastomers: at large strain, they show pronounced strain hardening.⁴⁷ Such strain hardening would obviously inhibit necking since any region of the film that thins locally would develop a locally higher modulus, and thus resist further thinning. The constitutive behavior used in our simulations ignores this, and therefore the plastic layers in the simulation are much more prone to non-homogeneous thinning than experiments. Indeed the most obvious failure of the constitutive model appears in simulations of stretching free-standing plastic layers. In simulations, such a layer develops a neck when the yield strength is exceeded, and the neck then locally thins to failure – behavior typical of plastic materials such as metals. In contrast, experimentally, a free standing plastic film (Fig. 2A) shows a single neck that does not thin to failure; instead it shows stable drawing behavior, testifying to the importance of strain hardening in capturing necking phenomena accurately.

It is useful to compare our simulations against linear stability analysis by Li and Suo.³⁶ A direct comparison is not possible since the constitutive equations used in that article are different from those used here. Nevertheless, a key point of that paper³⁶ is that whether necking occurs or not depends on the parameter EH_0/Kh_0 , where H_0 and h_0 are the thickness of the rubber and film respectively, E is the modulus of the rubber as measured in a uniaxial tensile experiment, and K is a measure of the yield strength. When EH_0/Kh_0 is significantly less than 1, necking is predicted.³⁶ If this parameter is much larger than 1, the rubber layer can suppress the necking behavior and therefore the plastic layer thins homogeneously. In our simulations, homogeneous deformation crosses over to necking when yield strength increases from 10 to 12.5 MPa. This corresponds to the parameter $EH_0/\sigma_y h_0$ decreasing from 2.89 to 2.31. These values are significantly higher than those from the linear stability analysis.³⁶ This discrepancy may be attributable to the different constitutive models used for the plastic layer here *vs.* in Li and Suo. Nevertheless, we do point out that while we have not seen non-homogeneous thinning at a rubber thickness of 860 microns, necking unquestionably happens when the rubber thickness is reduced to 100 microns (Fig. S2 (ESI[†])) as well as in simulations, (not shown). This is in qualitative agreement with the Li and Suo analysis³⁶ where

decreasing rubber layer thickness reduces the parameter $EH_0/\sigma_y h_0$, and therefore induces necking.

In summary then, for stretch-and-release induced wrinkles, as the yield stress of the face layers increases, stretching – and therefore subsequent wrinkling – becomes increasingly non-homogeneous. Combined with the conclusions of Section 4.1, we therefore conclude that stretch-and-release will generate uniform wrinkles only in a finite window of material properties. Stretch-and-release will produce non-homogeneous wrinkles if the yield strength is too high, and no wrinkles if the yield strength is too low.

5. Summary and conclusions

In summary, we have examined the surface wrinkling of composite films composed of an elastomeric layer sandwiched between two plastic face layers, an idea originally patented by Krueger *et al.*²⁹ The stretching of the initially smooth composite films leads to a geometric mismatch: since the plastic layers yield during stretching, the stress-free length of the plastic layers is longer than that of the elastomeric midlayer. Upon releasing, the film develops an internal stress, and the face layers undergo compression-induced buckling, resulting in a heavily wrinkled surface. High aspect ratio wrinkles – with the amplitude to wavelength ratio exceeding 0.4 – can be realized.

This paper points to numerous features of the stretch-and-release process that were not recognized previously.^{29–31} Specifically, plasticity of the face layers plays a key role at all stages of this process. The most obvious role, tensile yielding and irreversible increase in length during stretching, has already been recognized previously. In addition, simulations show (1) compressive yielding during release, (2) the formation of plastic hinges as wrinkles develop, and (3) non-uniform thinning during stretching (*i.e.* necking in the thickness direction) if the yield stress of the films is high or rubber thickness is small. Of these simulation predictions, our experiments unequivocally confirm plastic hinge formation, and strongly support in-plane yielding. We do not see thickness direction necking, at least at the single thickness examined in detail. However width-direction necking is clearly evident at small rubber thicknesses.

The constitutive models used here are very simple and are not able to tackle the full parameter space. For instance, one surprising experimental observation is that rubber thickness has only a weak effect on stretch-and-release; specifically, wrinkles appear even when the rubber “ought to be” too thin to induce yield of the plastic. We cannot address this in the current simulations because, perhaps due to the neglect of strain hardening effects, strong necking dominates the simulations when rubber thickness is small. Nevertheless, the simple constitutive model has illustrated features that are broadly relevant to thin film wrinkling situations where plastic deformation can occur. In particular, necking in tension and formation of plastic hinges are an inescapable consequence of yielding behavior, and will appear regardless of specific details such as the material used.

Taken together, the simulations suggest that stretch-and-release can produce uniform wrinkles only within a finite range of material properties. If the yield stress is too low, wrinkles are not expected since the face layers accommodate compression by in-plane yielding. If the yield stress is too high or the rubber thickness is too low, necks are expected and wrinkling is expected to become increasingly non-homogeneous over the surface. This is of obvious relevance to designing films that seek to exploit stretch-and-release to create wrinkled surfaces.

Acknowledgements

We thank Mr Takuya Inaba from Mitsui Chemicals for making the LLDPE films available, and Kraton Polymers for making the SEPS available for the research. We are grateful to Prof. Yadong Wang and Dr Kee-Won Lee for assisting with the use of their MTS tensile testing machine. Acknowledgment is made to the donors of the American Chemical Society Petroleum Research Fund for support of this research *via* grant #53386-ND7 to SV.

References

- 1 F. Brau, H. Vandeparre, A. Sabbah, C. Poulard, A. Boudaoud and P. Damman, *Nat Phys.*, 2011, **7**, 56–60.
- 2 X. Chen and J. W. Hutchinson, *Scr. Mater.*, 2004, **50**, 797–801.
- 3 Z. Y. Huang, W. Hong and Z. Suo, *J. Mech. Phys. Solids*, 2005, **53**, 2101–2118.
- 4 H. Q. Jiang, D. Y. Khang, J. Z. Song, Y. G. Sun, Y. G. Huang and J. A. Rogers, *Proc. Natl. Acad. Sci. U. S. A.*, 2007, **104**, 15607–15612.
- 5 D.-Y. Khang, J. A. Rogers and H. H. Lee, *Adv. Funct. Mater.*, 2009, **19**, 1526–1536.
- 6 J. Y. Chung, A. J. Nolte and C. M. Stafford, *Adv. Mat.*, 2011, **23**, 349–368.
- 7 E. P. Chan, E. J. Smith, R. C. Hayward and A. J. Crosby, *Adv. Mat.*, 2008, **20**, 711–716.
- 8 J. Y. Chung, J. P. Youngblood and C. M. Stafford, *Soft Matter*, 2007, **3**, 1163–1169.
- 9 J.-H. Lee, H. W. Ro, R. Huang, P. Lemaillet, T. A. Germer, C. L. Soles and C. M. Stafford, *Nano Lett.*, 2012, **12**, 5995–5999.
- 10 F. Greco, A. Bellacicca, M. Gemmi, V. Cappello, V. Mattoli and P. Milani, *ACS Appl. Mater. Interfaces*, 2015, **7**, 7060–7065.
- 11 Y. Li, S. Dai, J. John and K. R. Carter, *ACS Appl. Mater. Interfaces*, 2013, **5**, 11066–11073.
- 12 K. Efimenko, J. Finlay, M. E. Callow, J. A. Callow and J. Genzer, *ACS Appl. Mater. Interfaces*, 2009, **1**, 1031–1040.
- 13 N. Bowden, S. Brittain, A. G. Evans, J. W. Hutchinson and G. M. Whitesides, *Nature*, 1998, **393**, 146–149.
- 14 Y. Cao and J. W. Hutchinson, *J. Appl. Mech.*, 2012, **79**, 031019.
- 15 J. Huang, M. Juskiewicz, W. H. de Jeu, E. Cerda, T. Emrick, N. Menon and T. P. Russell, *Science*, 2007, **317**, 650–653.
- 16 D. P. Holmes and A. J. Crosby, *Phys. Rev. Lett.*, 2010, **105**, 038303.
- 17 L. Pocivavsek, R. Dellsy, A. Kern, S. Johnson, B. H. Lin, K. Y. C. Lee and E. Cerda, *Science*, 2008, **320**, 912–916.
- 18 S. Chatterjee, C. McDonald, J. Niu, S. S. Velankar, P. Wang and R. Huang, *Soft Matter*, 2015, **11**, 1814–1827.
- 19 N. Sridhar, D. J. Srolovitz and Z. Suo, *Appl. Phys. Lett.*, 2001, **78**, 2482–2484.
- 20 K. D. Hobart, F. J. Kub, M. Fatemi, M. E. Twigg, P. E. Thompson, T. S. Kuan and C. K. Inoki, *J. Electron. Mater.*, 2000, **29**, 897–900.
- 21 R. Huang and Z. Suo, *J. Appl. Phys.*, 2002, **91**, 1135–1142.
- 22 S. H. Im and R. Huang, *J. Appl. Math. Mech.*, 2005, **72**, 955–961.
- 23 E. P. Chan, K. A. Page, S. H. Im, D. L. Patton, R. Huang and C. M. Stafford, *Soft Matter*, 2009, **5**, 4638–4641.
- 24 P. J. Yoo and H. H. Lee, *Phys. Rev. Lett.*, 2003, **91**, 154502.
- 25 K. Srinivasan, G. Subbarayan and T. Siegmund, *Thin Solid Films*, 2012, **520**, 5671–5682.
- 26 J. Yin and X. Chen, *J. Phys. D: Appl. Phys.*, 2011, **44**, 045401.
- 27 Y.-P. Cao, X.-P. Zheng, F. Jia and X.-Q. Feng, *Comput. Mater. Sci.*, 2012, **57**, 111–117.
- 28 A. El Haitami, F. Bretagnol, P. Assuid, G. Petitet, S. Cantournet and L. Corte, *Langmuir*, 2013, **29**, 15664–15672.
- 29 D. L. Krueger, J. T. Bartusiak, T. P. Hanschen and K. M. Capik, *et al.*, *US Pat.*, 5691034, 1997.
- 30 Y. Hu, A. Hiltner and E. Baer, *Polym. Compos.*, 2004, **25**, 653–661.
- 31 A. Takei, L. Jin, H. Fujita, A. Takei, H. Fujita and L. Jin, *ACS Appl. Mater. Interfaces*, 2016, **8**, 24230–24237.
- 32 Y.-C. Chen and A. J. Crosby, *Adv. Mat.*, 2014, **26**, 5626–5631.
- 33 P. Van Puyvelde, S. Velankar and P. Moldenaers, *Curr. Opin. Colloid Interface Sci.*, 2001, **6**, 457–463.
- 34 P. J. Cole and C. W. Macosko, *J. Plast. Film Sheeting*, 2000, **16**, 213–222.
- 35 D. Langhe and M. Ponting, *Manufacturing and Novel Applications of Multilayer Polymer Films*, Elsevier, Amsterdam, 2016.
- 36 T. Li and Z. Suo, *Int. J. Solids Struct.*, 2006, **43**, 2351–2363.
- 37 B. J. Gurmessa and A. B. Croll, *Phys. Rev. Lett.*, 2013, **110**, 074301.
- 38 S. Pal, S. S. Damle, P. N. Kumta and S. Maiti, *Comput. Mater. Sci.*, 2013, **79**, 877–887.
- 39 S. Pal, S. S. Damle, S. H. Patel, M. K. Datta, P. N. Kumta and S. Maiti, *J. Power Sources*, 2014, **246**, 149–159.
- 40 J. Thunes, R. M. Miller, S. Pal, S. Damle, R. E. Debski and S. Maiti, *J. Biomech. Eng.*, 2015, **137**, 081012.
- 41 S. S. Damle, S. Pal, P. N. Kumta and S. Maiti, *J. Power Sources*, 2016, **304**, 373–383.
- 42 Trelis, 14.0 User Documentation, CSIMSOFT, 2012.
- 43 U. Ayachit, *The ParaView Guide: A Parallel Visualization Application*, Kitware, 2015.
- 44 M. R. Semler, J. M. Harris, A. B. Croll and E. K. Hobbie, *Phys. Rev. E: Stat., Nonlinear, Soft Matter Phys.*, 2013, **88**, 032409.
- 45 L. Jin, A. Takei and J. W. Hutchinson, *J. Mech. Phys. Solids*, 2015, **81**, 22–40.
- 46 J. Zang, X. Zhao, Y. Cao and J. W. Hutchinson, *J. Mech. Phys. Solids*, 2012, **60**, 1265–1279.
- 47 R. N. Haward, *Macromolecules*, 1993, **26**, 5860–5869.